GA–A26748

IMPLEMENTATION OF A NEW ATOMIC BASIS FOR THE He I EQUILIBRIUM LINE RATIO TECHNIQUE FOR ELECTRON TEMPERATURE AND DENSITY DIAGNOSTIC IN THE SOL FOR H-MODE PLASMAS IN DIII-D

by
J.M. MUNOZ BURGOS, O. SCHMITZ, E.A. UNTERBERG,
S.D. LOCH, and C.P. BALLANCE

JULY 2010

GENERAL ATOMICS

DISCLAIMER

GA–A26748

IMPLEMENTATION OF A NEW ATOMIC BASIS FOR THE He I EQUILIBRIUM LINE RATIO TECHNIQUE FOR ELECTRON TEMPERATURE AND DENSITY DIAGNOSTIC IN THE SOL FOR H-MODE PLASMAS IN DIII-D

by
J.M. MUNOZ BURGOS,* O. SCHMITZ,† E.A. UNTERBERG,‡
S.D. LOCH,¶ and C.P. BALLANCE¶

This is a preprint of a paper to be presented at the Nineteenth International Conference on Plasma Surface Interactions, May 24-28, 2010, in San Diego, California, and to be published in the *Proceedings.*

*Oak Ridge Institute for Science Education, Oak Ridge, Tennessee.
†Institut für Energieforschung-Plasmaphysik, Forschungszentrum Jülich, Association EURATOM-FZJ, Trilateral Euregio Cluster, Germany.
‡Oak Ridge National Laboratory, Oak Ridge, Tennessee.
¶Auburn University, Auburn, Alabama, Tennessee.

Work supported in part by
the U.S. Department of Energy
under DE-FC02-04ER54698, DE-AC05-06OR23100,
and DE-AC05-00OR22725

GENERAL ATOMICS PROJECT 30200
JULY 2010

GENERAL ATOMICS

ABSTRACT

Evaluating the ratio of selected helium lines allows for measurement of electron densities and temperatures. This technique is applied for L-mode plasmas at TEXTOR [O. Schmitz, *et al.*, Plasma Phys. Control. Fusion **50**, 115004 (2008)]. We report our first efforts to extend it to H-mode plasma diagnostics in DIII-D.

This technique depends on the accuracy of the atomic data used in the Collisional Radiative Model (CRM). We present predictions for the electron temperatures and densities by using recently calculated R-Matrix With Pseudostates (RMPS) and Convergent Close-Coupling (CCC) electron-impact excitation and ionization data. We include contributions from higher *Rydberg* states by means of the projection matrix. These effects become significant for high electron density conditions, which are typical in H-mode. We apply a non-equilibrium model for the time propagation of the ionization balance to predict line emission profiles from experimental H-mode data from DIII-D.

I. INTRODUCTION

He I line ratios are a powerful diagnostic tools at TEXTOR [1]. We wish to apply this method to obtain reliable measurements at the separatrix and Scrape-Off-Layer (SOL) regions. Emission calculations are based on the application of the CRM [2] and the quality of the atomic data employed in it. The main mechanisms for populating/de-populating excited states in the SOL are electron impact excitation and ionization. The atomic data used at TEXTOR [1] was obtained from Convergent Close Coupling (CCC) for some transitions, and normalized Born approximation for others. We employ new atomic data obtained by R-Matrix With Pseudostates (RMPS) [3], and CCC [4,5]. The use of non-perturbative methods makes a significant difference when calculating cross-sections [6], and rate coefficients [7] compared to those from perturbative methods. In our CRM we include coupling effects with higher *Rydberg* states (or cascades) by means of the projection matrix [8,9]. We implement a non-equilibrium ionization balance calculation to model the emission of the helium beam propagation along the vacuum chamber.

II. ATOMIC DATA

The RMPS calculation is described in detail by Ballance *et al.* [10], who shows the importance of including continuum coupling effects in the collision calculation. The electron-impact ionization rate coefficients were taken from CCC calculations [11].

In the Atomic Data Analysis Structure (ADAS) framework [12], the low n-shell atomic data is supplemented with data for the higher n-shells. The high n-shell data is called a projection matrix and is described by Summer *et al.* [8]. The electron-impact excitation data in the projection matrix consists of semi-empirical *Gaunt* factor calculations [13], and the electron-impact ionization data is calculated using the Exchange Classical Impact Parameter (ECIP) method [13]. Loch *et al.* [14] found that ECIP cross sections for the ionization of the excited states of neutral helium to be accurate when compared with non-perturbative calculations. By including the projection matrix in our calculations we construct our comprehensive CRM.

III. EQUILIBRIUM COLLISIONAL RADIATIVE MODEL

We apply the ADAS suite of codes in our modeling [12]. An atom/ion in the LS representation consists of a set of N-terms with radiative and collisional couplings. This system on an arbitrary excited i-term, can be represented by the time dependent equation [Eq. (1)] with the collisional processes (on the right hand side) included,

$$\frac{dn_{\mathrm{i}}}{dt} = -n_{\mathrm{i}}n_{\mathrm{e}}S_{\mathrm{i}}^{\mathrm{e}} + \sum_{\mathrm{j}>\mathrm{i}}\left(n_{\mathrm{j}}A_{\mathrm{j}\to\mathrm{i}} + n_{\mathrm{j}}n_{\mathrm{e}}q_{\mathrm{j}\to\mathrm{i}}^{\mathrm{e}} - n_{\mathrm{i}}n_{\mathrm{e}}q_{\mathrm{i}\to\mathrm{j}}^{\mathrm{e}}\right)$$

$$+\sum_{\mathrm{i}>\mathrm{j}}\left(n_{\mathrm{j}}n_{\mathrm{e}}q_{\mathrm{j}\to\mathrm{i}}^{\mathrm{e}} - n_{\mathrm{i}}A_{\mathrm{i}\to\mathrm{j}} - n_{\mathrm{i}}n_{\mathrm{e}}q_{\mathrm{i}\to\mathrm{j}}^{\mathrm{e}}\right) \quad , \tag{1}$$

where n_{e} is the free electron density, n_{i} is the i^{th} excited term being described, and n_{j} is the j^{th} population of any higher or lower term from i. We express Eq. (1) in the simplified form $\left(dn_{\mathrm{i}}/dt\right) = -C_{\mathrm{i,i}}n_{\mathrm{i}} + \sum_{\mathrm{j}\neq\mathrm{i}}C_{\mathrm{i,j}}n_{\mathrm{j}}$, with a diagonal loss terms of the collisional radiative matrix $C_{\mathrm{i,i}} = n_{\mathrm{e}}S_{\mathrm{i}}^{\mathrm{e}} + \sum_{\mathrm{j}\neq\mathrm{i}}\left(A_{\mathrm{i}\to\mathrm{j}} + n_{\mathrm{e}}q_{\mathrm{i}\to\mathrm{j}}^{\mathrm{e}}\right)$, and the non-diagonal gain terms of the collisional radiative matrix $C_{\mathrm{i,j}} = A_{\mathrm{i}\to\mathrm{j}} + n_{\mathrm{e}}q_{\mathrm{j}\to\mathrm{i}}^{\mathrm{e}}$. From a total of N terms we separate the number of metastable terms M (including the ground) and a number of ordinary terms $N - M$. The equilibrium solution (or quasi-steady-state approximation) for any n_{i} ordinary term is given by

$$n_{\mathrm{i}} = \sum_{j=1}^{N-M} C_{\mathrm{i,j}}^{(\mathrm{r})^{-1}}\left(-\sum_{k=1}^{M} n_{\mathrm{k}}C_{\mathrm{M+j,k}}\right) \quad , \tag{2}$$

where $C_{\mathrm{i,j}}^{(\mathrm{r})}$ is the reduced collisional radiative matrix which only includes the ordinary term elements and excludes the metastables.

In real atomic systems we have an infinite number of terms that asymptotically approach the ionization limit. To obtain a comprehensive solution, we include the higher *Rydberg* states into our collisional matrix. From the projection matrix we add the direct contribution $C_{\mathrm{i,j}}^{(\mathrm{dir})}$, and the higher *Rydberg* contributions $C_{\mathrm{i,j}}^{(\mathrm{indir})}$ [8,9]. Our comprehensive collisional matrix is given by $C_{\mathrm{i,j}} = C_{\mathrm{i,j}}^{\mathrm{dir}} + C_{\mathrm{i,j}}^{\mathrm{indir}}$. To calculate the line emission from the i^{th} term we use the integral expression for the intensity $I_{\mathbf{i}\to\mathbf{j}} = A_{\mathbf{i}\to\mathbf{j}}\int_a^b n_{\mathbf{i}}(x)dx$, where the integration is along the line of sight to account for the total emission. Since the gas is being introduced as a collimated beam we assume that the emission is localized. Thus, we approximate our local emission simply as $I_{\mathrm{i}\to\mathrm{j}} \approx A_{\mathrm{i}\to\mathrm{j}}n_{\mathrm{i}}\Delta x$, and our line ratio $R \approx \left(A_{\mathrm{i}\to\mathrm{j}}n_{\mathrm{i}}/A_{\mathrm{k}\to\mathrm{l}}n_{\mathrm{k}}\right)$, which we use to calculate

our different line ratios for a temperature and density grid that we use for our predictions. We have chosen the electron temperature sensitive (706.7 nm/728.3 nm), electron density sensitive (667.9 nm/728.3 nm), and electron temperature and density sensitive (706.7 nm/667.9 nm) line ratios. We use the following σ^2 minimization to determine our local values for electron temperature and density for the k^{th} experimental point

$$\sigma^2\left(T_e, N_e\right) = \left(1 - \frac{R_{T_e}^{\exp}}{R_{T_e}}\right)^2 + \left(1 - \frac{R_{N_e}^{\exp}}{R_{N_e}}\right)^2 + \left(1 - \frac{R_{T_e,N_e}^{\exp}}{R_{T_e,N_e}}\right)^2 \quad . \tag{3}$$

IV. NON-EQUILIBRIUM MODEL

There is another aspect to be considered when calculating line emission intensities. We use the approximation $I^{\lambda}_{i\to j} \approx A_{i\to j} n_i \Delta x = A_{i\to j} n^0 \left(n_i / n^0\right)\Delta x$ for calculating our line emissions, where n^0 is the helium neutral density, and n_i / n^0 is the normalized term population with respect to neutral density, and Δx is the line of sight length. When modeling line emissions, we must include time dependency since the time scales for ionization and recombination could be long. To calculate the time dependent ionization balance, ADAS considers an element **X** of nuclear charge z_o, the populations of the ionization stages are denoted by $n^z : z = 0,\ldots,z_0$. When considering the z ion stage we include in the calculation its own ionization ($S_{z\to z+1}$) and the ionization from the previous ion stage ($S_{z-1\to z}$). When talking about recombination we also only include those from the adjacent ion stages; $\alpha_{z\to z-1}$, $\alpha_{z+1\to z}$. The time dependence of the ionization stage populations is given by [12]

$$\frac{dn^z}{dt} = n_e S_{z-1\to z} n^{z-1} - \left(n_e S_{z\to z+1} + n_e \alpha_{z\to z-1}\right) n^z + n_e \alpha_{z+1\to z} n^{z+1} \quad . \tag{4}$$

Subject to the normalization condition $n^{Tot} = \sum_{z=0}^{z_0} n^z$, where n^{Tot} is the number density of ions of element **X** in any ionization stage. With the value for the velocity of the helium beam (v_b = 1.5 km/s), we get a nominal penetration distance of 1.5 m. Time effects must be included in our emission modeling. We compute the time it takes for the beam to reach the k^{th} radial position with $t_k = \left(r_0 - r_k\right)/\left(v_b\right)$. We also must know the initial conditions n_0^z or the conditions at the previous $k^{th} - 1$ point and so on. We assume that all the helium gas is on the ground state when entering the vacuum chamber.

V. RESULTS

We apply our equilibrium model without including the projection matrix (as in the stationary method (ST) in the TEXTOR model). We continue with the same new atomic data set but now including the projection matrix. We compare these results against the stationary method (ST) used as a diagnostic tool at TEXTOR [1]. Finally, we include the time dependent ionization balance for line emission calculations. Figures 1 and 2 show our predictions for calculating the electron temperatures and electron densities along the radial position of the vacuum chamber on TEXTOR (shot #101818). We apply our new model for line emission profiles reconstruction for shot #132741 at DIII-D, this way we explore the applicability of our model into H-mode.

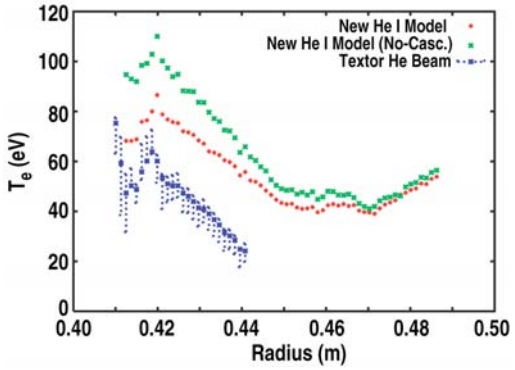

Fig. 1. Comparison of $T_e(r)$ profiles in discharge #101818 in TEXTOR. The x symbol represents the new model without cascades or high *Rydberg* states included, the + symbol represents the new model that includes the high *Rydberg* states, and the * symbol shows the data predictions from the TEXTOR model.

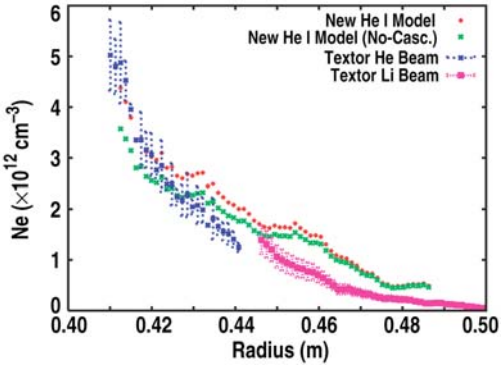

Fig. 2. Comparison of $N_e(r)$ profiles in discharge #101818 in TEXTOR. The x symbol represents the new model without cascades or high *Rydberg* states included, the + symbol represents the new model that includes the high *Rydberg* states, the * symbol shows the data predictions from the TEXTOR model, and the square symbol represents the Li beam diagnostics at TEXTOR.

A. T_e predictions

Figure 1 shows our predicted electron temperatures. Notice that for the higher temperature region the model with cascades (projection matrix included) shows significant differences from the non-cascades one. At the radial position $r < 0.42$ m we see differences up to 23 eV between the two, as well as roughly 20 eV differences between our new model and the TEXTOR predictions. We are able to extend the range of measurements by 4 cm in comparison to TEXTOR. When approaching the cooler region of the vacuum chamber (near the wall), both the bundled and unbundled models seem to agree. We get unphysical predictions of higher electron temperature values near the wall of the vacuum chamber. We suspect these predictions are caused by the long relaxation time for the triplet spin system of helium, and correction to this problem will be presented in a future publication. We see that for the $r < 0.42$ m region (Fig. 1), the predicted electron temperatures suffer a sudden drop. We suspect this behavior is due to experimental uncertainties in the low intensity experimental line emissions [1].

B. N_e predictions

For the case of electron density comparisons (Fig. 2), we get closer agreement between the bundled equilibrium model (with cascades) and the TEXTOR model. The maximum differences between the two are around 0.5×10^{12} cm^{-3}, but still within error bars of the TEXTOR model. For lower density predictions, we get some differences between the lithium beam data and our equilibrium model. We see differences of roughly 0.7×10^{12} cm^{-3} between the bundled and unbundled (no cascading) models for the higher density region. These results show that the inclusion of high *Rydberg* effects play an important role for building accurate helium line ratio diagnostics for H-mode plasma applications.

C. Emission profiles reconstruction

We calculated emission profiles by using experimental electron densities and temperatures from the *Thomson* scattering diagnostics for H-mode discharge #132741 in DIII-D. These emission profiles are constructed as a function of time and radial coordinate Z by considering a constant line of sight length (or no beam expansion). The purpose is to explore the region where we get the stronger line emission. We discuss two different cases, first the equilibrium case in which we may have a residual quantity of helium and how far into the separatrix we may get emission during H-mode.

The second case is the thermal beam (or gas puff) where we include the time dependent ionization balance for the emission as it propagates from the wall into the separatrix. We predict higher emission intensity at the separatrix for this case. We

calculate emission line intensity profiles for 667.9, 706.7, and 728.3 nm lines that are used for diagnostic (Figs. 3 through 8). Figures 3, 5, and 7 show the equilibrium case, while Figs. 4, 6, and 8 show the case of the thermal beam. The line emission diminishes as we move further into the separatrix with a distance of penetration of roughly 5 cm. We also see the emission diminishing during the transition from L-mode to H-mode. In Figs. 3 through 8, we see that the emission is much higher and very uniform in the regions of the separatrix and SOL for the thermal beam case compared it to the equilibrium model. This is the ideal behavior for diagnostics since this is the region we are interested in. We see the emission starts to drop more dramatically when transitioning into H-mode, but still it may be strong enough for diagnostic purposes. Experimental data is necessary in order to make a definite conclusion.

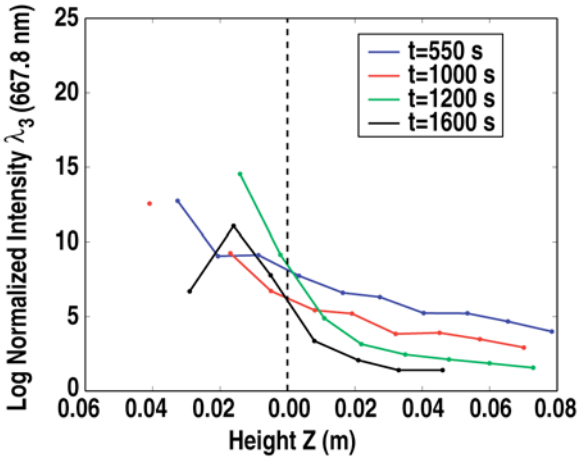

Fig. 3. H-mode transition for the modeled equilibrium line intensity emission profile as a function of radial position for the 667.9 nm line for discharge #132741 in DIII-D (RHS SOL, LHS Edge). Transition from L-mode (t = 550 ms) to H-mode (t = 1600 ms).

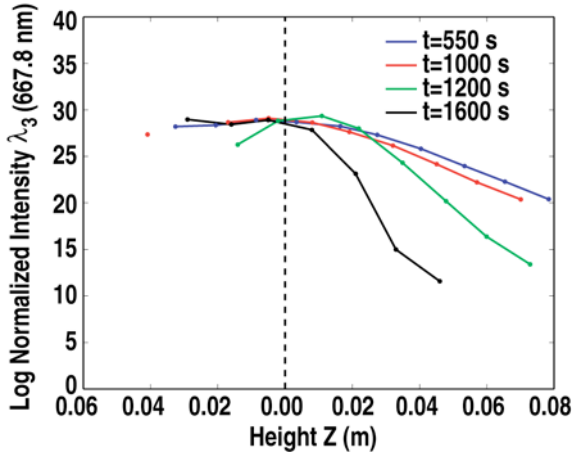

Fig. 4. H-mode transition for the modeled non-equilibrium line intensity emission profile as a function of radial position for the 667.9 nm line for discharge #132741 in DIII-D (RHS SOL, LHS Edge). Transition from L-mode (t = 550 ms) to H-mode (t = 1600 ms).

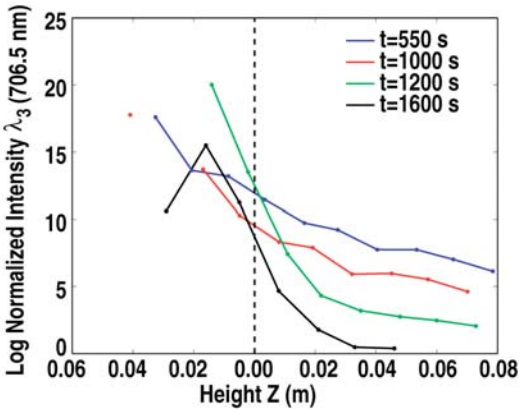

Fig. 5. H-mode transition for the modeled equilibrium line intensity emission profile as a function of radial position for the 706.7 nm line for discharge #132741 in DIII-D (RHS SOL, LHS Edge). Transition from L-mode (t = 550 ms) to H-mode (t = 1600 ms).

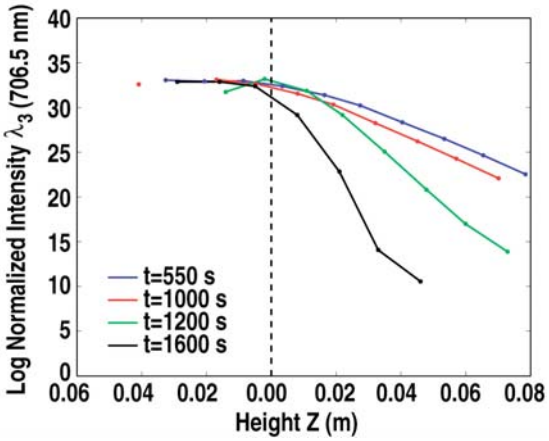

Fig. 6. H-mode transition for the modeled non-equilibrium line intensity emission profile as a function of radial position for the 706.7 nm line for discharge #132741 in DIII-D (RHS SOL, LHS Edge). Transition from L-mode (t = 550 ms) to H-mode (t = 1600 ms).

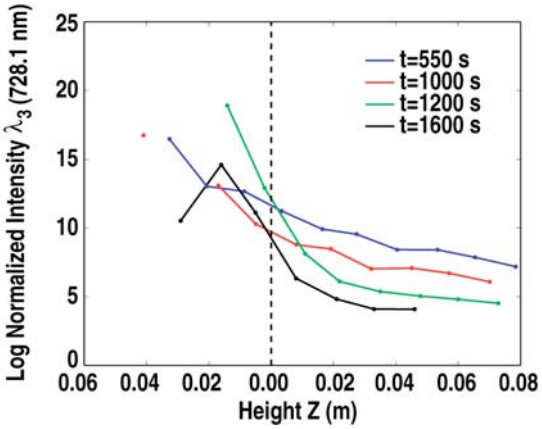

Fig. 7. H-mode transition for the modeled equilibrium line intensity emission profile as a function of radial position for the 728.3 nm line for discharge #132741 in DIII-D (RHS SOL, LHS Edge). Transition from L-mode (t = 550 ms) to H-mode (t = 1600 ms).

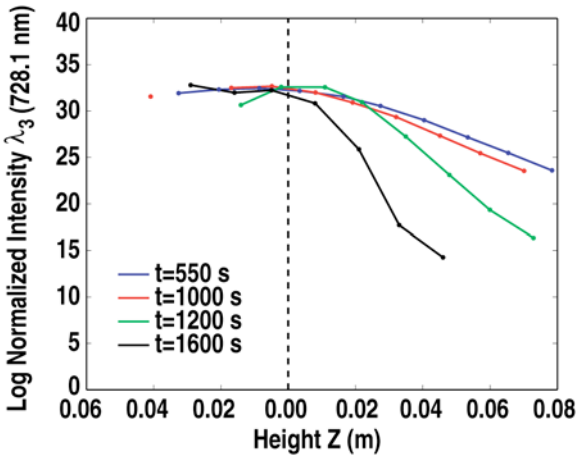

Fig. 8. H-mode transition for the modeled non-equilibrium line intensity emission profile as a function of radial position for the 728.3 nm line for discharge #132741 in DIII-D (RHS SOL, LHS Edge). Transition from L-mode (t = 550 ms) to H-mode (t = 1600 ms).

VI. CONCLUSIONS

We have assembled a comprehensive CRM, which includes the projection matrix to model high *Rydberg* contributions to our term populations in neutral helium. These are shown to have significant effects when predicting higher electron temperatures and densities which are present in H-mode plasmas. We have also included the most recent and experimentally-tested sets of electron impact excitation and ionization data. This makes us confident in our electron temperature and density predictions for localized gas helium sources. When modeling emission line intensity, the non-equilibrium model becomes necessary for describing the time evolution of the ionization balance. This model seems to be able to fulfill our goals for diagnostics at the separatrix and SOL regions for both L-mode and H-mode plasma conditions.

REFERENCES

[1] O. Schmitz, *et al.*, Plasma Phys. Control. Fusion **50**, 115004 (2008).

[2] D.R. Bates, *et al.*, Proc. R. Soc. A **267**, 297 (1962).

[3] K. Bartschat, Comput. Phys. Commun. **114**, 168 (1998).

[4] I. Bray and A.T. Stelbovics, Phys. Rev. A. **46**, 6995 (1992).

[5] D.V. Fursa and I. Bray, Phys. Rev. A **52**, 1269 (1995).

[6] D.C. Griffin, *et al.*, J. Phys. B: Atom. Mol. and Opt. Phys. **38**, L199 (2005).

[7] S.D. Loch, *et al.*, Plasma Phys. Control. Fusion **51**, 105006 (2009).

[8] H.P. Summers, *et al.*, Plasma Phys. Control. Fusion **48**, 263293 (2006).

[9] R.N. Badnell, *et al.*, Astronomy & Astrophysics **406**, 11511165 (2003).

[10] C.P. Ballance, *et al.*, Phys. Rev. A **74**, 012719 (2006).

[11] Y. Ralchenko, *et al.*, Atomic Data and Nuclear Data Tables **94**, 603 (2008).

[12] http://www.adas.ac.uk

[13] A. Burgess, H.P. Summers, Mon. Not. R. Astr. Soc. **174**, 345 (1976).

[14] S.D. Loch, *et al.*, Plasma Phys. Control. Fusion **51**, 105006 (2009).

ACKNOWLEDGMENTS

This work was supported in part by the US Department of Energy under DE-FC02-04ER54698, DE-AC05-06OR23100, and DE-AC05-00OR22725.